dissociation of the various complexes at a given pH:

$k_{HOAc}:k_{H(AC)^+} > 2000:1$ ($Cu(H_{-2}G_4)^-$; Table I)

$k_{HOAc}:k_{H(LS)^\pm} = 252:1$ ($Cu(H_{-1}G_4)$; Table II)

$k_{HOAc}:k_{H(LS)^\pm} = 275:1$ ($Cu(H_{-1}G_3)$; Table III)

$k_{HOAc}:k_{H(AC)^+} > 2000:1$ ($Cu(H_{-1}G_3)$; Table III)

$k_{HOAc}:k_{H(AC)^+} = 400:1$ ($Cu(H_{-2}G_3)^-$; Table III)

$k_{HOAc}:k_{H(LS)^\pm} > 2000:1$ ($Ni(H_{-2}G_3)^-$; Table IV)

The data prove the drastically reduced general-acid catalytic activity of H(LS) and $H(AC)^+$ as compared to that of HOAc. The fact that the pK_a values of HOAC and H(LS) are of the same size (4.6 and 4.8, respectively) and the finding that $k_{H(LS)^\pm} < 1$ M^{-1} s^{-1} (or even zero in some cases) makes H(LS), which is now commercially available, an attractive substitute for acetic acid as a buffer in kinetic studies. The role of H(LS) in the pH range 4.3–5.3 could be the same as that of MES in the pH range 5.7–6.7 (the application of the AC buffer as a substitute for the MES buffer is not advisable, since the base AC is of limited stability).

The main advantage of the 2,6-lutidine type buffers such as H(LS) is that, due to the absence of general-acid catalysis, the contribution of specific-acid catalysis and the contribution of general-acid catalysis produced by added acids HB can be determined more accurately.

Acknowledgment. Support by the Deutsche Forschungsgemeinschaft and by the Verband der Chemischen Industrie e.V. is gratefully acknowledged. Some of the buffers were kindly provided by Merck, Darmstadt, FRG.

Registry No. $Cu(H_{-2}G_3)^-$, 20160-84-3; $Cu(H_{-1}G_3)$, 12352-96-4; $Cu(H_{-2}G_4)^-$, 67180-35-2; $Cu(H_{-1}G_4)$, 15628-82-7; $Ni(H_{-2}G_3)^-$, 31011-65-1.

Contribution from the Institut für Physikalische und Theoretische Chemie, Universität Regensburg, D-8400 Regensburg, Federal Republic of Germany, and Institute of Inorganic Chemistry, University of Fribourg, CH-1700 Fribourg, Switzerland

Spectroscopic Studies of Cyclometalated Palladium(II) Complexes: Optical Absorption and Emission of Single-Crystal *cis*-Bis(benzo[*h*]quinolinato)palladium(II)

R. Schwarz,[†] G. Gliemann,*[,†] Ph. Jolliet,[‡] and A. von Zelewsky*[,‡]

Received February 29, 1988

The polarized optical absorption and emission spectra of single-crystal *cis*-bis(benzo[*h*]quinolinato)palladium(II) (≡[Pd(bhq)$_2$]) as functions of temperature (1.9 K ≤ T ≤ 60 K) are reported. The spectra and lifetime of the emission exhibit an unusual temperature dependence, indicating the luminescence to originate from several types of traps located energetically below the triplet exciton band of the crystal. At T = 1.9 K no energy transfer occurs between the traps, and the emission spectra are superpositions of the radiative deactivation of all traps. Raising the temperature depopulates the traps via the exciton band corresponding to the energetic depth of the traps. At T = 60 K only the deepest traps (ΔE = 780 cm^{-1}) are occupied and determine the luminescence.

Introduction

In a series of papers von Zelewsky, Balzani, and co-workers reported on the photochemical, photophysical, and electrochemical properties of several cyclometalated, homoleptic platinum(II) and palladium(II) complexes with C,N ligands.[1-6] The emission and absorption spectra of the corresponding glasses (at T = 77 K) and solutions (at room temperature) are distinctly structured, and the emission lifetimes are on the order of 10^{-6}–10^{-3} s. Depending on the central ions and/or the coordinating ligands the low-energy absorption processes are assigned to MLCT and LC transitions, respectively. Up to now for most of the cyclometalated complexes no detailed interpretations of their electronic structures have been available.

Recently Gliemann, von Zelewsky, and co-workers published the first spectroscopic study on single crystals of a cyclometalated d^8 complex.[7] In contrast to the glass, the crystalline [Pt(phpy)$_2$] (phpy = 2-phenylpyridine) exhibits one structureless phosphorescence band. The wavelength and the intensity of the emission depend as much on temperature as on the strength of an applied magnetic field, a behavior similar to that of other solid platinum(II) compounds.[8-14] By a method originally developed for single crystals of cyanoplatinates(II),[8-13] of binuclear $Pt_2(H_2P_2O_5)_4^{4-}$,[14] and of several $[W(CO)_5X]$ compounds[15,16] the character of the low-energy optical transitions and the energetic order as well as the symmetry of the emitting states could be assigned.

The purpose of this paper is to get further details on the electronic states of single-crystal cyclometalated d^8 complexes. We report on the temperature dependence of the polarized optical absorption and emission of single-crystal [Pd(bhq)$_2$]. A qualitative model of the electronic properties of the crystalline compound is established to rationalize the observed behavior.

Experimental Section

Single crystals of [Pd(bhq)$_2$] were prepared according to ref 1 and 5. The needle-shaped crystals used for the spectroscopic measurements had a size of 3 × 0.1 × 0.05 mm^3.

The polarized crystal emission was measured with a liquid helium bath

[†] Universität Regensburg.
[‡] University of Fribourg.

(1) Chassot, L.; Müller, E.; von Zelewsky, A. *Inorg. Chem.* **1984**, *23*, 4289.
(2) Maestri, M.; Sandrini, D.; Balzani, V.; Chassot, L.; Jolliet, P.; von Zelewsky, A. *Chem. Phys. Lett.* **1985**, *122*, 375.
(3) Bonafede, S.; Ciano, M.; Bolletta, F.; Balzani, V.; Chassot, L.; von Zelewsky, A. *J. Phys. Chem.* **1986**, *90*, 3836.
(4) Chassot, L.; von Zelewsky, A.; Sandrini, D.; Maestri, M.; Balzani, V. *J. Am. Chem. Soc.* **1986**, *108*, 6084.
(5) Chassot, L.; von Zelewsky, A. *Inorg. Chem.* **1987**, *26*, 2814.
(6) Balzani, V.; Maestri, M.; Melandri, A.; Sandrini, D.; Chassot, L.; Cornioley-Deuschl, C.; Jolliet, P.; Maeder, U.; von Zelewsky, A. Photochemistry and Photophysics of Coordination Compounds. In *Proceedings of the Seventh International Symposium*; Yersin, H., Vogler, A., Eds.; Springer-Verlag: Berlin, Heidelberg, New York, 1987. Maestri, M.; Sandrini, D.; Balzani, V.; von Zelewsky, A.; Jolliet, P. *Helv. Chim. Acta* **1988**, *134*, 71.
(7) Bär, L.; Gliemann, G.; Chassot, L.; von Zelewsky, A. *Chem. Phys. Lett.* **1986**, *123*, 264.
(8) Gliemann, G.; Yersin, H. *Struct. Bonding* **1985**, *62*.
(9) Hidvegi, I.; von Ammon, W.; Gliemann, G. *J. Chem. Phys.* **1982**, *76*, 4361.
(10) Hidvegi, I.; von Ammon, W.; Gliemann, G. *J. Chem. Phys.* **1984**, *80*, 2837.
(11) Dillinger, R.; Gliemann, G.; Pfleger, H. P.; Krogmann, K. *Inorg. Chem.* **1983**, *22*, 1366.
(12) Biedermann, J.; Wallfahrer, M.; Gliemann, G. *J. Lumin.* **1987**, *37*, 323.
(13) Schwarz, R.; Lindner, M.; Gliemann, G. *Ber. Bunsen-Ges. Phys. Chem.* **1987**, *91*, 1233.
(14) Bär, L.; Gliemann, G. *Chem. Phys. Lett.* **1984**, *108*, 14.
(15) Dillinger, R.; Gliemann, G. *Chem. Phys. Lett.* **1985**, *122*, 66.
(16) Dillinger, R.; Gliemann, G. *Z. Naturforsch.* **1986**, *41A*, 1071.

0020-1669/89/1328-0742$01.50/0

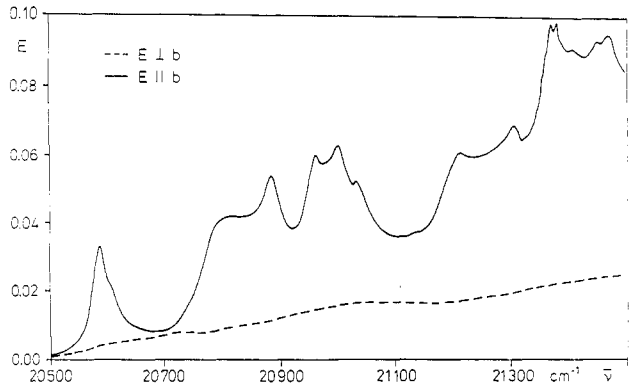

Figure 1. Polarized low-energy absorption spectra of single-crystal $[Pd(bhq)_2]$ at T = 10 K (crystal thickness 50 μm).

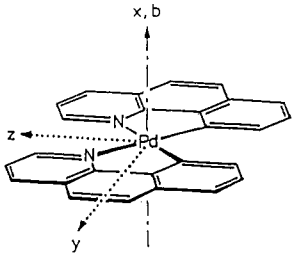

Figure 2. Schematic representation of the complex $[Pd(bhq)_2]$. x, y, and z denote the molecular axes; b denotes the crystallographic b axis.

cryostat of a superconducting magnet system (Oxford Company, SM 4). The emitted light was analyzed by a Spex double-grating monochromator (Czerny–Turner mounting) and was detected by an EMI S20 photomultiplier. The 364-nm line and the 488-nm line of an argon ion laser (Coherent, Innova 90) were used as excitation sources for the CW spectra, and the 435-nm line of a cavity dumped dye laser system (dye stilben 3) was used for the lifetime measurements.[17] For the excitation spectra a dye laser (Lambda Physik FL 2000; dye Cumarin 307) was used. The apparatus and methods for studying the polarized absorption has been described in ref 18.

All luminescence measurements were performed with the electric field vector of the exciting light parallel to the crystallographic b axis.

Results

Figure 1 shows the low-energy section of the polarized absorption spectra of single-crystal $[Pd(bhq)_2]$ at T = 10 K. The $\mathbf{E}\|b$ spectrum was recorded with the electric field vector $\mathbf{E}$ of the light parallel to the crystallographic b axis, which coincides with the needle axis of the crystal (cf. Figure 2). The absorption band of lowest energy (band maximum at $\bar{\nu}$ = 20 574 cm^{-1}, half-width $\Delta\bar{\nu} \approx 40$ cm^{-1}) has an asymmetrical shape. Assuming that the molar concentration of $[Pd(bhq)_2]$ in the crystal equals that of $[Pt(bhq)_2]$ (c = 3.68 mol L^{-1} [19]), the extinction coefficient of this band can be estimated as $\epsilon \approx 2$ L mol^{-1} cm^{-1}. Variation of the temperature between T = 10 K and room temperature influences neither the band energies nor the band intensities of the $\mathbf{E}\|b$ polarized absorption spectrum. The $\mathbf{E}\perp b$ polarized absorption spectrum is less intense than the $\mathbf{E}\|b$ spectrum and exhibits no distinct structure (cf. Figure 1).

In Figure 3 the unpolarized excitation spectrum (detection wavenumber $\bar{\nu}_{det}$ = 19 700 cm^{-1}) at T = 7 K is shown. This spectrum is not corrected for instrument response. All features of the strongest band in the excitation spectrum are in good correspondence with those of the $\mathbf{E}\|b$ absorption band of lowest energy. The wavenumber of the maximum is 20 580 cm^{-1}, the half-width is ~50 cm^{-1}, and the excitation band also has an asymmetrical form. At the low-energy flank of the dominating excitation band some small bands appear, indicating very weak absorptions between 20 100 and 20 500 cm^{-1}. Variation of the detection wavelength does not change the excitation spectrum.

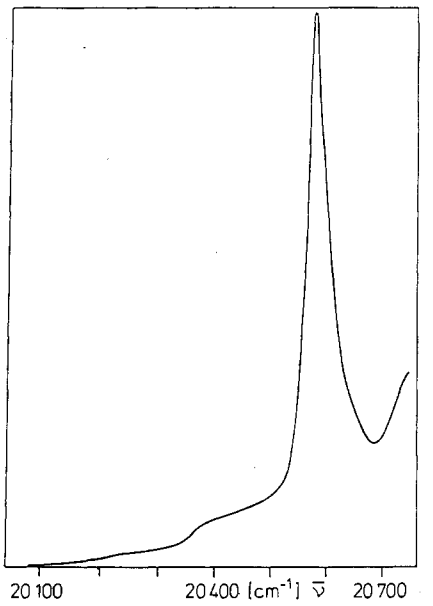

Figure 3. Unpolarized excitation spectrum of single-crystal $[Pd(bhq)_2]$ at T = 7 K (detection wavelength λ_{det} = 507.6 nm ($\bar{\nu}$ = 19 700 cm^{-1})).

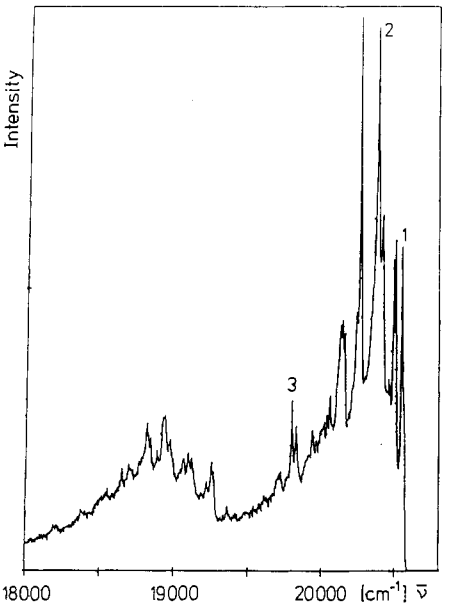

Figure 4. $\mathbf{E}\|b$ polarized emission spectrum of single-crystal $[Pd(bhq)_2]$ at T = 1.9 K (λ_{exc} = 364 nm).

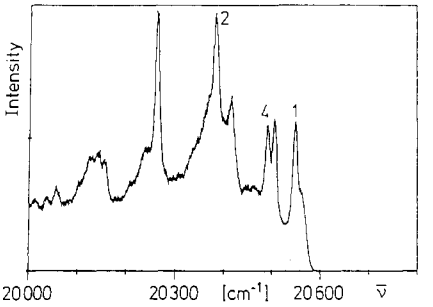

Figure 5. $\mathbf{E}\|b$ polarized high-energy emission spectrum of single-crystal $[Pd(bhq)_2]$ at T = 1.9 K (λ_{exc} = 364 nm).

Figure 4 presents the $\mathbf{E}\|b$ polarized emission spectrum at T = 1.9 K. The excitation wavelength is λ_{exc} = 364 nm. For $\mathbf{E}\perp b$ polarization a very similarly shaped but a factor of ~1.5 less intense emission spectrum results. In their high-energy ranges the spectra exhibit intense, sharp fine structures without a progression. As an example Figure 5 shows the high-energy section of the $\mathbf{E}\|b$ emission spectrum. The half-widths of the sharp lines

(17) von Ammon, W. Thesis, Universität Regensburg, 1981.
(18) Tuszynski, W.; Gliemann, G. *Ber. Bunsen-Ges. Phys. Chem.* **1985**, *89*, 940.
(19) Bernardinelli, G.; von Zelewsky, A. To be submitted for publication.

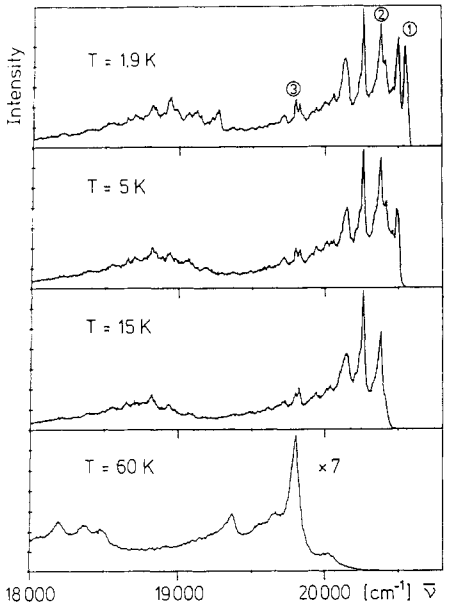

Figure 6. E‖*b* polarized emission spectra of single-crystal [Pd(bhq)$_2$] at different temperatures (λ_{exc} = 364 nm).

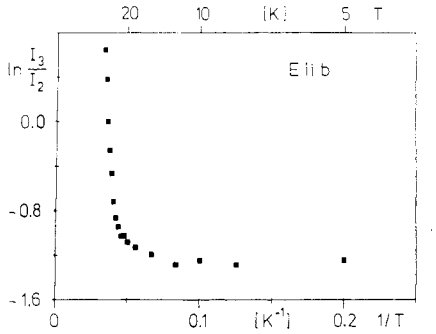

Figure 7. Logarithmic plot of the emission intensity ratio I_3/I_2 versus $1/T$. I_3 and I_2 are the intensities of the emission lines 3 and 2, respectively.

are ~15 cm^{-1}. Between the high-energy shoulder of peak 1 (at $\bar{\nu}$ = 20 555 cm^{-1}) and the absorption maximum of lowest energy there is an energy gap of $\Delta\bar{\nu} \approx$ 19 cm^{-1}. On the other hand, the emission spectra overlap strongly (by $\Delta\bar{\nu} \approx$ 500 cm^{-1}) with the excitation spectrum (cf. Figures 3 and 5).

The behavior of the E‖*b* polarized emission spectrum in the temperature range between T = 1.9 and 60 K is shown in Figure 6. The intensities of the spectra at T = 1.9, 5, and 15 K are comparable. With a temperature increase from T = 1.9 to 15 K the sharp lines at the high-energy end of the emission spectrum vanish successively one by one, beginning with the line of highest energy. Simultaneously with these lines some emission peaks at lower energy (satellites) disappear. The intensities and half-widths of the remaining peaks are not changed by this temperature variation. Further increase of temperature yields a red shift and a smoothing of the emission spectra. The most intense maximum of the 60 K spectra is by $\Delta\bar{\nu}$ = 760 cm^{-1} lower in energy than peak 1 of the 1.9 K spectra, and its energy position is identical with that of the intense peak 3 of the 1.9 K spectra. Raising the temperature from T = 15 to 60 K reduces the integral emission intensity by a factor of ~8, whereas the ratio of the intensities, $I_\parallel/I_\perp \approx$ 1.5, remains constant.

In order to demonstrate the extinction of the sharp emission lines with increasing temperature, Figure 7 shows the plot of ln (I_3/I_2) versus $1/T$. The intensity I_3 of peak 3 is independent of temperature and has been used as a reference to minimize the experimental error. Between T = 1.9 and ~20 K the value of ln (I_3/I_2) is constant within the experimental error, indicating that the emission intensity I_2 of peak 2 is independent of temperature. Further increase of temperature causes a decrease of I_2. The slope

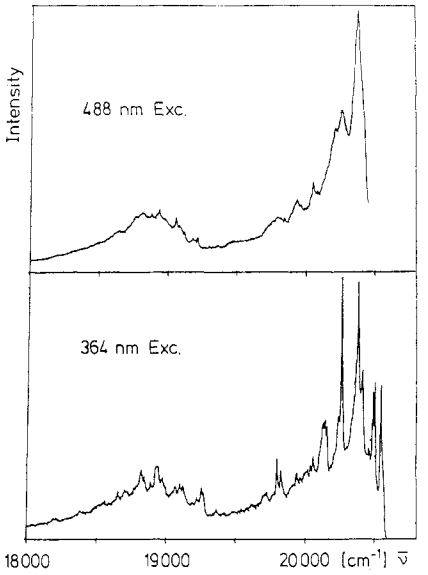

Figure 8. Comparison of the E‖*b* polarized emission spectra of single-crystal [Pd(bhq)$_2$] at λ_{exc} = 488 and 364 nm (T = 1.9 K).

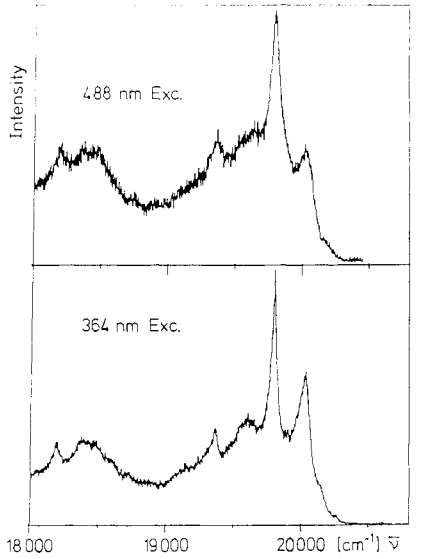

Figure 9. Comparison of the E‖*b* polarized emission spectra of single-crystal [Pd(bhq)$_2$] at λ_{exc} = 488 and 364 nm (T = 50 K).

of the plot in the temperature range 20 K ≤ T ≤ 30 K is ~−254 K.

In Figures 8 and 9 the emission spectra with excitation wavelengths λ_{exc} = 364 and 488 nm are compared at T = 1.9 and 50 K, respectively. The radiation with λ_{exc} = 488 nm (upper parts of Figures 8 and 9) is 75 cm^{-1} lower in energy than the emission peak 1 and coincides energetically with the emission peak 4 in the 1.9 K spectrum with 364-nm excitation (cf. Figure 5). At T = 1.9 K the spectrum with λ_{exc} = 488 nm exhibits a coarse feature similar to that of the 364-nm spectrum, but the fine structures are distinctly different. All sharp lines lower in energy than peak 4 are missing in the 488-nm spectrum, and all satellites recognizable in the 488-nm spectrum do not appear in the 364-nm spectrum. A very different behavior has been observed at higher temperatures, as shown by Figure 9 for T = 50 K. There, the emission spectra are independent of the excitation wavelength.

The decay rates of the polarized emission have been measured at different temperatures. At T = 1.9 K the decay curves are monoexponential and have a slope yielding a lifetime of τ = 85 μs. This value is independent of the direction of polarization and has been found at every emission wavelength. (Because of the very low intensity the lifetime has been measured with a band-pass of ~25 cm^{-1}.) When the temperature is raised, all peaks that can be deleted by increasing temperature display a distinct

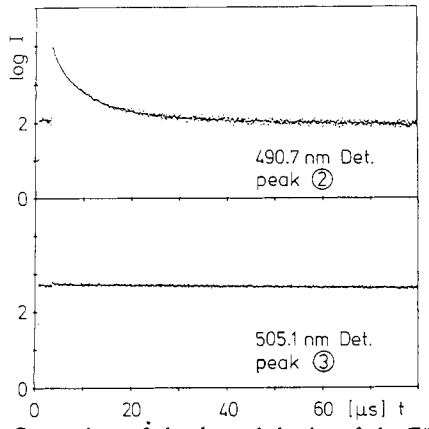

Figure 10. Comparison of the decay behavior of the $\mathbf{E}\|b$ polarized emission spectra of single-crystal $[Pd(bhq)_2]$ at λ_{det} = 490 nm ($\bar{\nu}$ = 20408 cm^{-1}) and 505.1 nm ($\bar{\nu}$ = 19798 cm^{-1}) (λ_{exc} = 364 nm, T = 35 K).

nonexponential decay, whereas the intensities of the remaining peaks maintain their monoexponential decay with τ = 85 μs, as shown in Figure 10.

The emission spectra of single-crystal $[Pd(bhq)_2]$ cannot be influenced by homogeneous magnetic fields ($H \leq 6$ T).

Discussion

Structural reports on the $[Pd(bhq)_2]$ crystal have not been available until now. Because of the similar molecular structure, crystal morphology, and double refraction of $[Pd(bhq)_2]$ and $[Pt(bhq)_2]$ the structure type of the platinum compound is assumed to be valid also for the $[Pd(bhq)_2]$ crystal.[19] As shown in Figure 2, the molecular x axis is perpendicular to the plane of the complex and coincides with the crystallographic b axis, which is parallel to the needle axis of the single crystal. The symmetry of the Pd ion with its nearest surroundings can be approximated by the point group C_{2v} (double group C'_{2v}). The 2-fold rotation axis (molecular z axis) is the line of intersection of the two molecular symmetry planes.

The π-electron system of the ligand bhq is comparable to that of the heterocycle *o*-phen(*o*-phen = *o*-phenanthroline). Therefore, the symmetries of the HOMO and the LUMO of bhq can be assigned to the irreducible representations b_1 and a_2 of the C_{2v} group, respectively.[20] By linear combination of the HOMO's of the two ligands of a complex a stabilized hybrid MO of symmetry b_1 and a destabilized MO of symmetry a_2 result. Linear combination of the two LUMO's yields also a stabilized b_1 hybrid and a destabilized a_2 hybrid. Thus, the HOMO and the LUMO of the pair $(bhq)_2$ have a_2 and b_1 symmetry, respectively.

As has been analyzed for planar platinum(II) complexes with C,N coordination, the energetic order of the metal d orbitals in the ligand field is[12,13,21]

$$1a_1(x^2) < 1b_1(xz),\ 1a_2(xy) < 2a_1(y^2 - z^2) \ll 1b_2(yz)$$

For symmetry reasons this ligand field splitting is expected to be preserved if Pt(II) is substituted by Pd(II).

Balzani et al. assigned the low-energy transition in the absorption spectrum of the dissolved $[Pd(bhq)_2]$ to an intraligand $\pi\pi^*$(LC) transition.[6] To reconcile this assignment with the energy level system, the HOMO a_2 of the ligand system is higher in energy than the metal state $2a_1(y^2 - z^2)$, whereas the LUMO b_1 of the ligand system is lower in energy than the metal state $1b_2(yz)$. Thus, the HOMO a_2 and LUMO b_1 of the ligand system constitute, respectively, the HOMO and LUMO of the total complex. For symmetry reasons an admixture of the metal d state $1a_2(xy)$ to the HOMO a_2 is expected, yielding a partial metal character of the HOMO.

When electron interaction is taken into account, the electron ground-state configuration of a single complex turns into the term

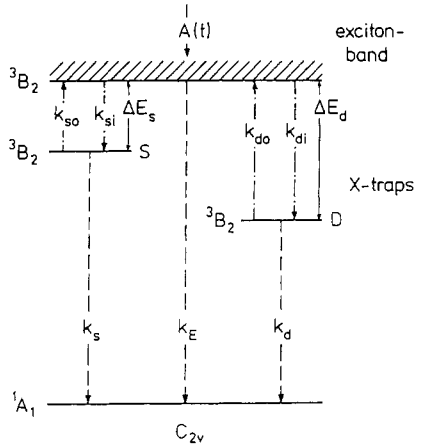

Figure 11. Proposed energy level diagram of single-crystal $[Pd(bhq)_2]$ (S, shallow X-trap; D, deep X-trap).

$^1A_1$; the first excited configuration ($a_2 \rightarrow b_1$) forms the two terms $^1B_2$ and $^3B_2$. By the spin–orbit coupling due to the heavy metal Pd(II) an increase of the intersystem crossing rate but no energetically considerable removal of the $^3B_2$ degeneracy is expected.

In the crystal the terms $^1B_2$ and $^3B_2$ form exciton bands. For the interpretation of the optical properties of single-crystal $[Pd(bhq)_2]$ we assume the existence of X-traps with sharp energy levels, which are located energetically below the $^3B_2$ exciton band. The X-traps are due to $[Pd(bhq)_2]$ complexes, which are disturbed by impurities or defects in the crystal. Free ligands and Pd(IV) complexes can be ruled out as traps, since the emission of both species is expected at energies higher than that of the Pd(II) complex.[6] Furthermore, between T = 1.9 and 77 K the emission spectrum of the dissolved Pd(II) complex shows no change of energy, shape, and lifetime, and it exhibits no fine structure, which could be assigned to species corresponding to the different traps in the crystal state.[6,22] In Figure 11 the resulting energy level diagram is shown. For the sake of clearness only two different types of X-traps are represented, a shallow trap with stabilization energy ΔE_s and a deep trap stabilized by ΔE_d. Corresponding models have been developed to describe the optical properties of single crystals of organic compounds.[23-28]

The asymmetrical low-energy absorption band (cf. Figure 1) can be assigned to the transition from the ground state $^1A_1$ to the $^3B_2$ exciton band. Since this transition is spin forbidden, the very small extinction coefficient can be understood. The half-width of the absorption band is only an upper limit of the width of the exciton band. The strongest band of the excitation spectrum (cf. Figure 3) corresponds to absorption processes into the $^3B_2$ exciton band, whereas the weaker bands can be traced back to an absorption by different types of X-traps.

The optical emission at low temperatures is expected to originate from the radiative deactivation of X-traps. Subsequent to the excitation (λ_{exc} = 364 nm) the exciton band is populated by relaxation processes of rate $A(t)$. Then the energy can be transferred rapidly via the exciton band to the X-traps with rates k_{si}, $k_{di} \gg k_E$ (cf. Figure 11). Since the energy transfer between the traps proceeds via the exciton band, at T = 1.9 K such an energy transfer can be precluded and the emission is the superposition of the luminescence of all X-trap types. The sharp lines in the high-energy section of the emission spectra represent different 0–0 transitions, respectively one per X-trap type. With regard to the definition of the X-traps as weakly disturbed $[Pd(bhq)_2]$ complexes it is evident that all X-traps have, within the

(20) Heilbronner Straub. *Hückel-Molecular Orbitals*; Springer-Verlag: Berlin, Heidelberg, New York, 1966.
(21) Isci, H.; Mason, W. R. *Inorg. Chem.* **1975**, *14*, 905.
(22) Schwarz, R.; Gliemann, G. Unpublished results.
(23) Fayer, M. D.; Harris, C. B. *Phys. Rev. B* **1974**, *9*, 748.
(24) Shelby, R. M.; Zewail, A. H.; Harris, C. B. *J. Chem. Phys.* **1976**, *64*, 3192.
(25) Weinzierl, G.; Friedrich, J. *Chem. Phys. Lett.* **1981**, *83*, 204.
(26) Komada, Y.; Yamauchi, S.; Hirota, N. *J. Chem. Phys.* **1984**, *82*, 1651.
(27) Güttler, W.; von Schütz, J. U.; Wolf, H. C. *Chem. Phys.* **1977**, *24*, 150.
(28) Vala, M.; Baiardo, J.; Wierzbicki, A.; Trabjberg, I. *Chem. Phys.* **1987**, *116*, 221.

experimental error, the same emission lifetime. The value τ = 85 μs is much lower than that of the free ligand ($\tau > 10^5$ μs) and that of the complex in glasses (τ = 2600 μs) at T = 77 K[6] and 7 K.[22] These differences are probably caused by different spin-orbit couplings due to a weak admixture of the metal orbital $1a_2(xy)$ to the HOMO of the complex and by an intercomplex coupling in the crystal, respectively.

Raising the temperature depletes the X-trap states and populates the exciton band. According to the strong temperature dependence of the detrapping rates k_{so}, k_{do} and to the distinct stabilization energies ΔE_s, ΔE_d the depopulation of the different X-trap types starts at different temperatures. With increasing temperature first the shallow X-traps are deactivated ($k_{so} \neq 0$, $k_{do} \approx 0$) and the corresponding 0-0 transitions (and their vibronic satellites) of the emission spectra vanish. The simultaneous loss of the monoexponential character of the decay and the reduction of the emission lifetime of the shallow-trap states are accomplished by the competing mechanisms of detrapping and trapping. At further temperature increase to $T \approx 60$ K thermal equilibrium is established between all X-traps, with the exception of the deepest one ($\Delta E_d \approx 780$ cm^{-1}), and the exciton band. For this reason the 60 K emission spectra consist only of the deep-trap emission. The observed reduction of the integral emission intensity between T = 5 and 60 K is probably due to the inefficiency of the system in transferring the total excitation energy via the exciton band to the deep traps, and there exists rather a nonradiative deactivation with a temperature-dependent rate.

To describe the temperature dependence of the detrapping processes, a quantitative model developed by Fayer and Harris[23,24] can be applied. In this model the detrapping rate k_{so} of a shallow trap varies with temperature as $k_{so} = k_{so}^0 e^{-\Delta E_s/kT}$ with ΔE_s being the stabilization energy. If there exist deeper traps (stabilization energies ΔE_d) coupled to the shallow traps via the exciton band, then the logarithmic plot of the intensity ratio

$$\frac{I_d}{I_s} = \frac{N_d}{N_s} \frac{k_s + k_{so}^0 e^{-\Delta E_s/kT}}{k_d + k_{do}}$$

versus the reciprocal temperature $1/T$ is composed of two parts. N_d and N_s are the numbers of the traps, and I_d and I_s represent the emission intensities of the deep and the shallow traps, respectively. At temperatures too low to depopulate the shallow traps and the deep traps (k_{so}, k_{do} = 0; $k_s \approx k_d$), the intensity ratio is constant and reflects the ratio of the numbers of deep and of shallow traps. In the temperature range that allows the detrapping of the shallow traps but not of the deep traps ($k_{so} \gg k_s$; k_{do} = 0), ln (I_d/I_s) varies as $-\Delta E_s/kT$. The slope of the plot of ln (I_d/I_s) versus $1/T$ yields the trap depth ΔE_s. Experiments of this kind with crystalline organic compounds have been reported in ref 25-28.

If the emission lines labeled by the numbers 2 and 3 in Figure 4 are assigned to shallow traps and deep traps, respectively, the graph in Figure 7 is in agreement with the theoretical predictions. From Figure 7 the value of the stabilization energy ΔE_s can be calculated as $\sim$177 cm^{-1}. That harmonizes well with the experimental energy gap of $\Delta\bar{\nu} < 204$ cm^{-1} between the emission peak 2 and the low-energy absorption band.

With excitation wavelength λ_{exc} = 488 nm a selective excitation of X-traps of type 4 results. At T = 1.9 K a thermally activated energy transfer from these traps into the exciton band is suppressed and, therefore, all traps of other type remain in their electronic ground state. For this reason the emission spectrum consists only of the trap 4 emission and it differs distinctly from the 1.9 K spectrum with UV excitation. Raising the temperature causes an efficient detrapping of the X-traps of type 4. The corresponding energy is transferred rapidly via the exciton band and finally localized at X-traps again. At T = 50 K all traps with the exception of the deepest one ($\Delta E \approx 780$ cm^{-1}) are in thermal equilibrium with the exciton band and, therefore, the 50 K emission spectrum is assigned to originate from the deepest traps.

Acknowledgment. This research has been supported by the Deutsche Forschungsgemeinschaft, the Fonds der Chemischen Industrie, and the Swiss National Science Foundation.

Contribution from the Christopher Ingold Laboratories, University College London, 20 Gordon Street, London WC1H 0AJ, England

Electronic, Infrared, Raman, and Resonance Raman Spectra of the Dirhodium Tetracarboxylate Complexes $Rh_2(O_2CR)_4(PPh_3)_2$ (R = H, CH_3, C_2H_5, C_3H_7)

Robin J. H. Clark* and Andrew J. Hempleman

Received May 10, 1988

The electronic spectra of the series of complexes $Rh_2(O_2CR)_4(PPh_3)_2$ (R = H, CH_3, C_2H_5, C_3H_7) are characterized by a strong absorption ($\lambda_{max} \approx 380$ nm) of essentially $\sigma(Rh_2) \rightarrow \sigma^*(Rh_2)$ character. Excitation within the contour of this band leads to resonance Raman spectra that are dominated by a band progression in ν(RhRh). Both resonance Raman and Raman (514.5 nm) spectra have been obtained for the complexes with R = H, C_2H_5, C_3H_7, and these are compared to those previously reported for $Rh_2(O_2CCH_3)_4(PPh_3)_2$. While ν_1 (ν(RhRh)) occurs at 292 $\pm$ 7 cm^{-1} over all four complexes, the band attributed to the totally symmetric ν(RhO) vibration, ν_2, is shown to be strongly dependent on the mass of the R group, occurring at 402, 338, 310, and 289 cm^{-1} for the complexes with R = H, CH_3, C_2H_5, and C_3H_7, respectively. The intensity ratio $I(\nu_2)/I(\nu_1)$ and the length of the overtone progressions in ν_2 are shown to be dependent upon the wavenumber separation ν(RhO) - ν(RhRh). FTIR spectra (3500-40 cm^{-1}) are also assigned.

Introduction

For dimetal tetracarboxylates of the type $M_2(O_2CR)_4L_2$, changes in the carboxylate bridging ligand usually have little effect upon ν(MM) if the axial ligands either are absent or are kept constant. Thus, for the series $Mo_2(O_2CR)_4$ (R = H, CH_3, C_2H_5, C_3H_7, C_6H_5, C_6H_{11}, CF_3, CH_2Cl, $CHCl_2$, CCl_3) ν(MoMo) is found in the range 406-395 cm^{-1} [1-8] and for the series $Ru_2(O_2CR)_4Cl$ (R = H, CH_3, C_2H_5, C_3H_7) ν(RuRu) is found in the range 339-327 cm^{-1}.[6,9] This relative insensitivity of ν(MM) to change of R is a reflection of the lack of mixing between the R group and M-M symmetry coordinates as well as of the small

* To whom correspondence should be addressed.

(1) Cotton, F. A.; Norman, J. G., Jr.; Stults, B. R.; Webb, T. R. *J. Coord. Chem.* **1976**, *5*, 217.
(2) Hutchinson, B.; Morgan, J.; Cooper, C. B., III; Mathey, Y.; Shriver, D. F. *Inorg. Chem.* **1979**, *18*, 2048.
(3) Bratton, W. K.; Cotton, F. A.; Debeau, M.; Walton, R. A. *J. Coord. Chem.* **1971**, *1*, 121.
(4) Clark, R. J. H.; Hempleman, A. J.; Kurmoo, M. *J. Chem. Soc., Dalton Trans.* **1988**, 973.
(5) Ketteringham, A. P.; Oldham, C. *J. Chem. Soc., Dalton Trans.* **1973**, 1067.
(6) San Filippo, J., Jr.; Sniadoch, H. J. *Inorg. Chem.* **1973**, *12*, 2326.

0020-1669/89/1328-0746$01.50/0